Soft Matter

Dynamic Article Links

Cite this: *Soft Matter*, 2012, **8**, 9553

www.rsc.org/softmatter

PAPER

Bioinspired templates for the synthesis of silica nanostructures

Natalia Hassan,†[a] Armando Soltero,[b] Danilo Pozzo,[c] Paula V. Messina[d] and Juan M. Ruso*[a]

Received 31st May 2012, Accepted 16th July 2012
DOI: 10.1039/c2sm26263k

Herein we report a facile method for the preparation of hierarchical silica nanostructures through a biomimetic approach. Toward this goal, a protein-directed approach has been proposed to template silica into 3D architectures through a hydrogel matrix formed from physically cross-linked fibrinogen. The hydrogel matrix has tunable physicochemical properties based on the thermal unfolding of the main domains of the protein. The network structures of the gels that are obtained are quite similar but differ in the mean pore size and rheological properties. These nanopores are then filled with silica precursors, under acidic conditions, where the condensation reaction is initiated. The protein hydrogel template is subsequently removed by calcination. The final materials show two different topologies. The origin of these two topologies lies on the anisotropic shape of the fibrinogen, driving stochastic interactions with the inorganic precursor and thus generating sponge-like (normal interactions) and polygonal fiber (parallel interactions) architectures.

1. Introduction

Natural materials consist of just a few constituent elements that provide a wide range of systems with multiple functions. These may also serve as a source of bio-inspiration to synthesize minerals, materials and devices, simplifying many of our day-to-day functions.[1] In diatoms and sponges the production of a wide variety of nanopatterned silica structures in a genetically controlled manner is directed by proteins.[2] In order to be able to synthesize new bio-inspired materials it is important to first perform thorough investigations of structure–function relationships in natural biological materials. These must also address new questions and challenges that are motivated by recent discoveries. Recent years have seen a significant change in this situation. For example, the notion that proteins are simply three-dimensional, compact objects has been recently questioned.[3] While proteins need to keep their structures thermally stable, native folds often display an ability to undergo large amplitude conformational changes that are critical for proper function.[4] Indeed, the possibility that proteins may be better characterized by fractal geometries, rather than as compact three-dimensional objects, has been recently proposed.[3] In the case of protein surfaces, a fractal dimension of 2.1 to 2.4 is widely accepted. Nevertheless, the fractal dimension of the protein itself based on several estimates has been argued to lie near 2.5.[5] In this sense, it appears that when viewed as fractals, proteins exhibit an unexpected universal behavior[6] than can be parameterized. Also the distribution of hydrophobicity and polarizability in the protein interior follow a fractal scaling.[7]

Fibrous proteins such as keratins, silks, collagen or fibrin also exhibit impressive mechanical properties as well as biocompatibility. Therefore, these proteins are under study to be used as biomaterials and scaffolds for tissue engineering.[8] For example, soft protein matrices that mimic brain are neurogenic, stiffer matrices that mimic muscle are myogenic and comparatively rigid matrices that mimic collagenous bone prove to be osteogenic.[9] In this context, the integration of inorganic materials with biological systems may offer solutions needed to accomplish task such as reproducibly manipulating and controlling assembly at the molecular level. Thus, bioinorganic assemblies, such as aggregates of nanoparticles and filamentous bacteriophages (phage), have shown many potential applications in areas such as cancer targeting, bio-materials/electronics and stem cell tissue engineering.[10] Consequently, mimicking biological processes has become an important method for the fabrication of sophisticated architectures. Therefore, the controlled assembly of nanoscaled units into complex hierarchical structures could be an effective strategy to obtain higher functionality and performance while exploring bioinspired morphosynthesis.[7]

Fibrinogen is a complex multidomain protein whose major function is to form fibrin clots that prevent the loss of blood upon vascular injury. Bovine fibrinogen (340 kDa) is an elongated protein that is approximately 45 nm long (and has an

[a]*Soft Matter and Molecular Biophysics Group, Department of Applied Physics, University of Santiago de Compostela, Santiago de Compostela, 15782, Spain. E-mail: juanm.ruso@usc.es; Tel: +34 981563100*
[b]*Departamento de Ingeniería Química, Universidad de Guadalajara, Guadalajara, Jalisco, 44430 Mexico*
[c]*Department of Chemical Engineering, University of Washington, Seattle, WA 98195, USA*
[d]*INQUISUR-CONICET, Department of Chemistry, Universidad Nacional del Sur, (8000) Bahía Blanca, Argentina*
† Current address: Laboratoire Physico-chimie des Electrolytes, Colloides et Sciences Analytiques (PECSA), Université Pierre et Marie Curie, 75252 Paris, France.

approximate diameter of 5 nm). Fibrinogen is a disulfide-linked dimer of three polypeptide chains, Aα, Bβ, and γ. The NH_2 terminal portions of the six chains are linked together in the central region of the molecule by 11 disulfide bonds forming a small globular domain, the so-called disulfide knot, in the center.[11,12] The C termini of each of the three chains end in globular domains. Those corresponding to the Bβ and γ chains are located at the ends of the molecule. Cleavages in all three chains then yield two D domains and one E domain. The E domain consists of the NH_2-terminal regions of α-, β-, and γ-chains held together by disulfide bonds. The majority of the D region is formed by the C-terminal portions of the β- and γ-chains folded into similar structures. The COOH-terminal portion of each fibrinogen Aα chain forms a compact αC-domain attached to the bulk of the molecule with a flexible αC-connector. In addition, fibrinogen shows a unique characteristic in its folding. According to the current view, two αC-domains in fibrinogen interact intramolecularly with each other and with the central region of the molecule. In contrast, in fibrin they switch to an intermolecular interaction to form αC-polymers. This structural organization drives the fibrin assembly process and promotes cell adhesion and migration through RGD sequences.[13] Recent studies have focused on the complexation of fibrinogen with ligands, including surfactants and drugs, and on their adsorption behavior at different interfaces.[14–17] These studies use a combination of experimental techniques (*e.g.* equilibrium dialysis, difference spectroscopy, microcalorimetry, zeta potential, static and dynamic light scattering and circular dichroism) to enable the complete characterization and understanding of the physicochemical phenomena involved in these interactions. Despite the biological importance and interesting applications of this protein, the gel formation has only been studied in the presence of thrombin. Through proteolytic cleavage, this enzyme converts fibrinogen into insoluble strands of fibrin and drives gelation. Despite some initial work,[18–20] the possibility of using these proteins directly to design nanomaterials remains virtually untapped.

In previous work we have studied the effect of composition on the morphology, swelling, and rheological properties of ovalbumin gels. This new study represents a step forward in which the aim is twofold; first, the primary objective is to determine how temperature and pH affect the viscoelastic properties and topology of fibrinogen hydrogels. Second, we aim to determine the catalytic role of fibrinogen hydrogels and their potential to act as templating agents in the formation of siliceous structures. This approach has great potential for material design because it is based on an environmentally friendly green protocol that is also a less expensive and readily available route for the synthesis of nanostructured materials.

2. Materials and methods

Materials

Bovine plasma fibrinogen, fraction I, type IV, was purchased from Sigma and was used without further purification. For the preparation of fibrinogen hydrogels, protein solutions of different concentrations, ranging from 10×10^{-3} to 40×10^{-3} g L^{-1}, were incubated in a water bath at 37 °C for 30 min. After that, the fibrinogen solutions were adjusted to pH 3 by addition of 0.1 M HCl. Later, the solutions were incubated again in a water bath at either 37 °C or 70 °C for another 2 hours. The procedure for forming fibrinogen hydrogels at pH 8 was different. Here, the protein was dissolved in a buffer solution of 50 mM glycine and the pH was adjusted with NaOH. The hydrogels were then incubated in a water bath at 37 °C for 30 min and after this time the solutions were again incubated at either 37 or 70 °C for another 2 hours. All chemical reagents were of analytical grade, and solutions were made using doubly distilled and degassed water.

Synthesis of mesoporous silica

Here, 0.2 g of fibrinogen was dissolved in 20 g of distilled water and 3.067 g of sodium silicate was added at room temperature with magnetic stirring, giving a clear solution. To this reaction mixture, 6.1349 g of 37% HCl was quickly added with vigorous magnetic stirring. The resulting gel mixture was stirred for 1 day at room temperature and subsequently heated for 12 hours at 100 °C in an autoclave to increase the degree of silanol condensation. The solid product was then filtered and dried at 100 °C. The product was calcined in air under static conditions at 550 °C.

Conductivity measurements

Conductivities were measured using a Kyoto Electronics conductometer model CM-117 with a K-121 cell type. The cell constant was determined using KCl solutions following the procedure suggested by Monk. All measurements were performed in a Polyscience model PS9105 temperature controlled water bath. The protein was dissolved in water and the pH was adjusted to pH 3.0 with 0.1 M HCl. For samples at pH 8.0, the protein was dissolved in a buffer consisting of 50 mM glycine and the pH was adjusted with NaOH. The protein solutions were then heated at a linear rate of 40 °C h^{-1}.

Rheology

Rheological experiments were performed on a Bohlin CS-10 stress-controlled rheometer. A Couette geometry (cup 27.5 mm diameter, height 35 mm, gap 5 mm) and a bob of the Mooney type were used. The cell was heated by a reservoir of fluid circulating from a Julabo thermostated bath. The sample was equilibrated for at least 20 min prior to each experiment. Both steady and dynamic rheological experiments were performed at each temperature. Dynamic frequency sweep measurements were performed in the linear viscoelastic regime of the samples, as determined by dynamic stress-sweep measurements. For the steady-shear experiments, an equilibration time of 90 s was given at each shear stress.

Field emission scanning electron microscopy (FE-SEM)

Field emission scanning electron microscopy (FE-SEM) was performed using a FE-SEM ULTRA PLUS. This instrument operates in high vacuum enabling the collection of high resolution images (0.8 nm at 30 kV) and low voltage in samples without coating (0.02 V to 30 kV, continuously adjusted in steps of

10 volts). The magnification of the images ranged from 12–1 000 000× and the sizes of the openings that were used were 7.5 μm, 10 μm, 20 μm, 30 μm, 60 μm and 120 μm. Local charging was compensated by injection of nitrogen gas.

X-ray powder diffraction

Powder X-ray diffraction (XRD) data were collected with a Philips PW 1710 diffractometer with Cu-Kα_α radiation (λ = 1.5418 Å) and a graphite monochromator operated at 45 kV; 30 mA and 25 °C.

3. Results and discussion

Hydrogel characterization

It was previously reported that temperature, the presence of denaturants, ionic strength, protein concentration and pH are all important factors in the controlled aggregation and gelation of proteins. Consequently, we have considered the effect of some of these factors on the change in conformation of fibrinogen molecules and their self-assembly.[21] Fig. 1 shows the influence of temperature, pH and fibrinogen concentration on the ionic conductivity of the solutions. Changes in the slopes are related to the threshold of gel formation. It was found that, both increasing the pH as well as increasing the concentration of fibrinogen in the solution led to a significant increase in the ionic conductivity of the samples. Heat-induced gelation of globular proteins has a very strong temperature dependence because it involves denaturation as the first step, which is a highly cooperative process characterized by a large activation energy. Increasing the temperature led to faster evolution of the system and higher final values of the gel conductivity in agreement with previous findings.[22] In the case of hydrogels formed at pH 3.0, with the same protein content, there are no significant differences in conductivities throughout the temperature range. In contrast, for samples at pH 8.0 a significant enhancement in the ionic conductivity of the hydrogel can be observed with increasing temperature, mainly at lower temperatures. Visual inspection of the samples reveals that proteins coagulate at pH 8.0 and the solutions become cloudy and not useful for rheological analysis. Consequently, solutions at pH 3.0 were chosen as models to form fibrinogen hydrogels.

As indicated in the Experimental methods section, fibrinogen solutions were incubated at either 37 or 70 °C during gelation. These temperatures were chosen based on our previous work on thermal denaturation of fibrinogen.[17] Differential scanning calorimetry analysis has revealed three endothermic peaks for fibrinogen. Two narrow and symmetrical peaks located at 53 and 94 °C have been attributed to the denaturation of the end D and central E fragments of fibrinogen respectively, while the small and broad peak located at 77 °C has been related to the denaturation of the C-terminal of the Aα chains. Thus, fibrinogen gels synthesized at 37 °C maintain their three domains intact while for those synthesized at 70 °C the end D domains, the largest in the protein, are denatured.

The next consideration involves the analysis of the mechanical properties of the gels. For this purpose, rheological measurements were performed on the hydrogels. Fig. 2 shows the elastic modulus (G') obtained from oscillatory stress deformation sweeps measured as a function of fibrinogen concentration (C). Experiments were performed at a frequency (ω) of 10 rad per s and at a temperature of 25 °C, for gels prepared at 37 °C (a) or at 70 °C (b). These experiments were performed in order to identify the linear viscoelastic region (LVR). The LVR is the deformation range where G' is independent of deformation (γ%).[23] The breakdown of the hydrogel structure is denoted by the rapid decline of G' at large deformations. For hydrogel samples prepared at 37 °C (Fig. 2a), it is evident that the LVR is dependent on the fibrinogen concentration. For concentrations between 10 and 15 g L^{-1}, the linear viscoelastic region extends up to strain values around 0.1%. When the fibrinogen concentration is increased, the strain-independent region shifts towards even higher values (1%). This increase in the LVR may be due to increases in the cross-linking density that augment the resistance of hydrogel samples against deformation. Upon increasing the fibrinogen concentration, G'' (not shown) also increased in a similar way as the elastic modulus (G'). However, G' values became considerably greater in magnitude than G'' values.

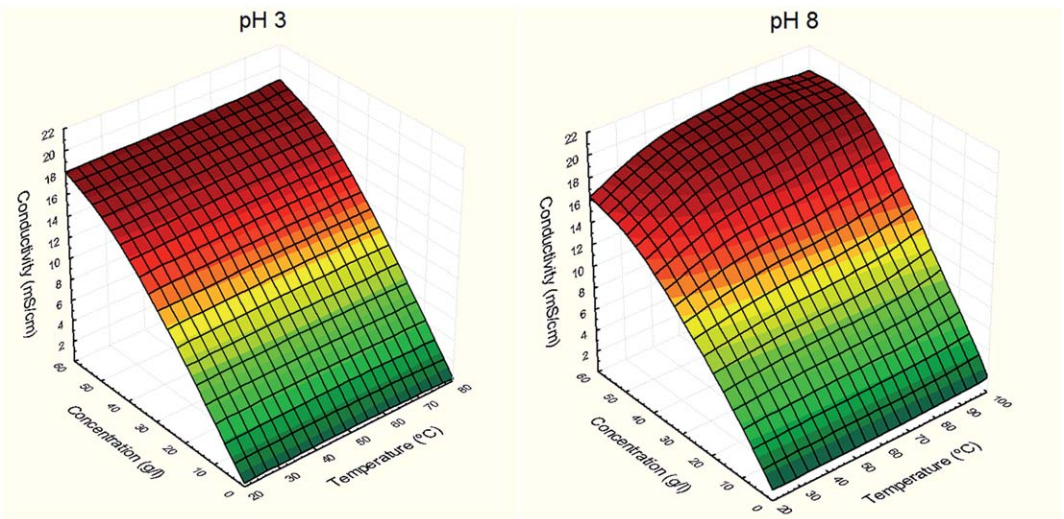

Fig. 1 Plots of electrical conductivity of fibrinogen hydrogels against temperature and concentration at pH 3.0 (left) and pH 8.0 (right).

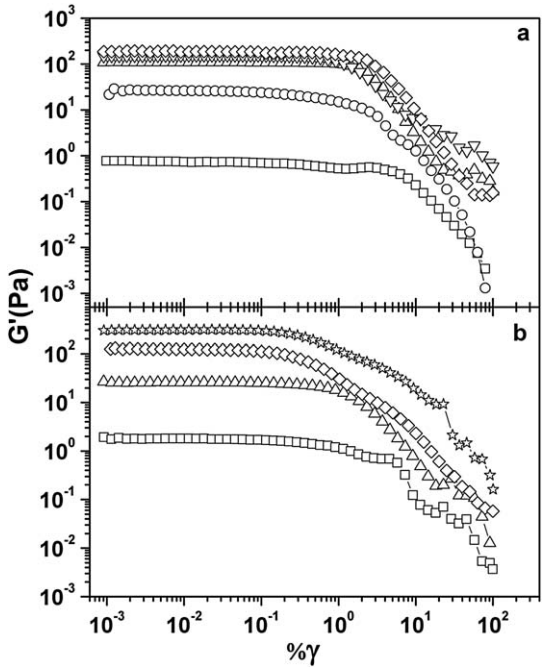

Fig. 2 Strain sweeps made at 10 rad per s and 25 °C as a function of fibrinogen concentration (g L^{-1}): (□), 10; (○), 15; (△), 20; (▽), 25; (◇), 30 and (☆), 40. Synthesized at (a) 37 °C and (b) 70 °C.

Consequently the gel hardness is dependent on the protein concentration and, accordingly, the cross-linking density. On the other hand, hydrogels prepared at 70 °C (Fig. 2b) exhibited similar behavior to that observed in samples prepared at 37 °C. However, the LVR spans only up to deformations around 0.1% for all the concentrations studied.

Fig. 3a and b show the elastic and viscous moduli that are obtained when frequency sweep experiments at different concentrations are performed. The applied strain was 0.025% and the measurement temperature was 25 °C. For the sample with a concentration of 10 g L^{-1} that was prepared at 37 °C (Fig. 3a), both G' and G'' are somewhat dependent on frequency. This behavior is similar to that observed in weak viscoelastic gels of lamellar liquid crystals that are formed by anionic surfactants in water *e.g.*, didodecyldimethylammonium bromide (DDAB) and aerosol OT (AOT),[24,25] food biopolymer gels[26] and in myofibrillar proteins of fish.[27] At higher concentrations (Fig. 3a), samples showed true gel-like behavior where both G' and G'' are frequency independent. It is evident in this figure that, the dynamic moduli values increase as the concentration increases and G' values also become increasingly greater in magnitude than G'' values. The relative increase in G' over G'' causes the gels to become stronger and harder and this is demonstrated by the decrease in tan δ (dissipation capacity). This could be due to the increase in the cross-linking density with increasing protein concentrations. On the other hand, samples prepared at 70 °C (Fig. 3b) are independent of frequency over all fibrinogen concentrations that were studied. This means that, for protein concentrations higher than 10 g L^{-1}, hydrogels prepared at a temperature of 70 °C are more loosely cross-linked than those prepared at 37 °C.

The variations in the log–log plot of the elastic modulus as a function of fibrinogen concentration and temperature are shown

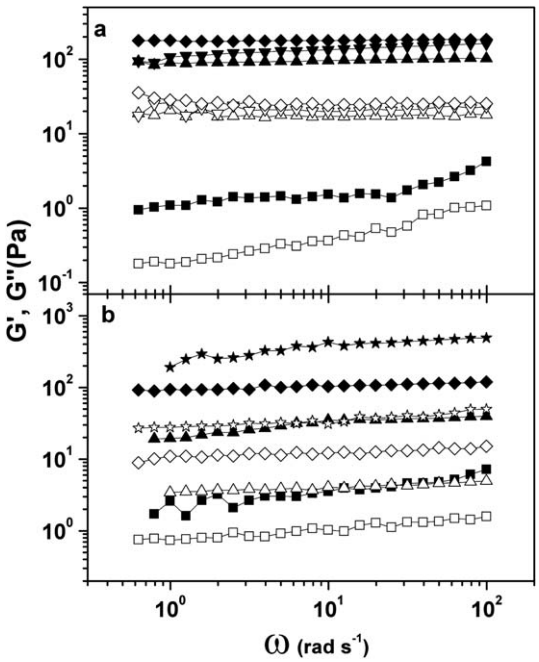

Fig. 3 Elastic G' (closed symbols) and loss G'' (open symbols) moduli as a function of frequency for different fibrinogen concentrations (g L^{-1}): (□), 10; (○), 15; (△), 20; (▽), 25; (◇), 30 and (☆), 40. Synthesized at (a) 37 °C and (b) 70 °C. Experiments were performed at an applied strain of 0.02% and 25 °C.

in Fig. 4a for samples prepared at 37 °C (squares) and at 70 °C (circles). Data were obtained at $\omega = 10$ rad per s, at an applied strain of 0.025% and at a measurement temperature of 25 °C. It is observed in this figure that hydrogels prepared at 37 °C show larger G' values than those prepared at 70 °C. This suggests that samples prepared at 37 °C are more highly cross-linked than those prepared at 70 °C. On the other hand, for both datasets the

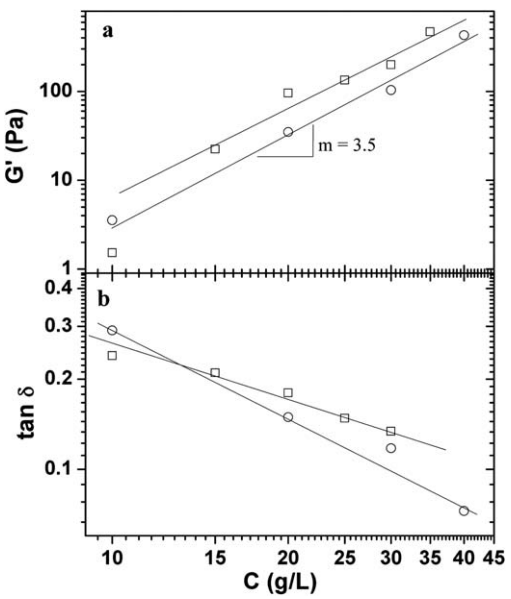

Fig. 4 Elastic modulus G' (a) and tan δ (b) values as a function of fibrinogen concentration for samples prepared at 37 °C (squares) and 70 °C (circles) at $\omega = 10$ rad per s and 25 °C.

slopes are almost the same ($m \sim 3.5$). Clark and Ross-Murphy[28] reported a power law relationship between G' and the concentration of protein and polysaccharide gels corresponding to C^2 at high C/C_0 ratios, where C_0 is the critical concentration. Below the critical concentration values macroscopic gels are not formed. They also reported that larger power law exponents are usually found in other gelling biopolymers for C/C_0 values lower than 10. A model for densely cross-linked actin proteins and entangled solutions was also proposed by MacKintosh *et al.*[29] They showed, for entangled solutions, the elastic modulus scaled with concentration as

$$G' \propto C^A \quad (1)$$

with $A = 2.2$. Similar power law exponent values were reported for hydrogels based on F-actin,[29] coarse fibrin networks[30] and for oligopeptides.[31] The slope of 3.5 obtained for our system is higher than that predicted by eqn (1) but lower than that reported for hydrogels (4.5) based on oligomeric electrolytes.[32] Fig. 4b shows log–log plots of the variation of tan δ (G''/G') values with fibrinogen concentration and the preparation temperature, 37 (squares) or 70 °C (circles). For both samples, tan δ values decrease as protein concentrations increase. This decrease indicates that the hydrogel is becoming harder and less mechanical dissipation can occur at high protein concentrations. The value of the slope for samples prepared at 37 °C is also smaller than for samples prepared at 70 °C. This means that, for concentrations higher than 10 g L^{-1}, the elasticity of samples prepared at 70 °C becomes greater in magnitude than that of samples synthesized at 37 °C with increasing protein concentration.

To summarize, when the concentration of protein is less than 10 g L^{-1} the mechanical behavior of the gels is similar. However, at higher protein concentrations the crosslinking density and mechanical stiffness of gels synthesized at 37 °C, where the native structure is maintained, are higher than that of samples prepared at 70 °C. It was previously reported that fibrinogen–fibrinogen interactions occur through αC chains to form networks.[33,34] When the protein maintains its native structure, alpha domains have larger degrees of freedom that favor entanglement and enhance cross-linking.

Another interesting feature in the rheology of the gels is the temperature dependence. Fig. 5 shows the dependence of the elastic modulus (G') as a function of temperature during the gelation process for samples prepared at 37 °C (a) and 70 °C (b) with different fibrinogen concentrations. Measurements were performed at a frequency of 10 rad per s and an applied strain of 0.025%, so that the probe deformation is within the linear viscoelastic regime. All the samples exhibit elastic behavior, $G' > G''$, over all of the studied temperatures. For samples prepared with a protein concentration of 10 g L^{-1} at 37 °C, the elastic modulus is temperature independent up to around 45 °C where a rapid increase of six orders of magnitude is observed and a constant value is eventually reached. This increase in G' allows us to identify the transition temperature (T_G) of the sample. For samples with concentrations higher than 10 g L^{-1}, T_G shifts to 57 °C and the maximum value of G' decreases with increasing concentration. On the other hand, the increase of G' above T_G for concentrated samples is only about two orders of magnitude.

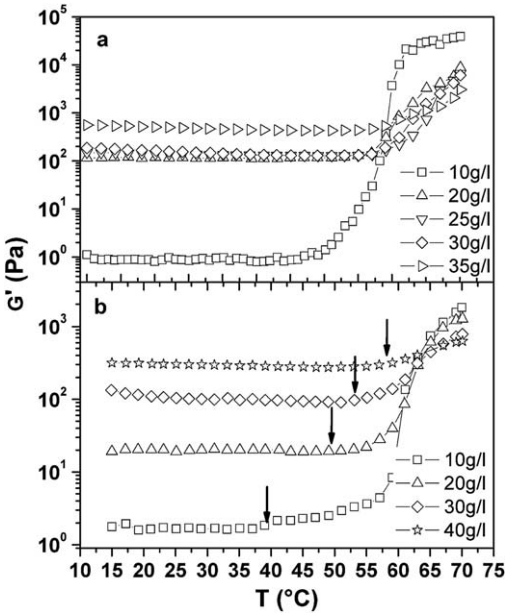

Fig. 5 Temperature dependence of the elastic modulus G' for samples prepared at 37 °C (a) and 70 °C (b) for different fibrinogen concentrations (g L^{-1}): (□), 10; (△), 20; (▽), 25; (◇), 30; (▷), 35 and (☆), 40. Experiments were performed at an applied strain of 0.025% and at a frequency $\omega = 10$ rad per s.

This increase is much lower than that of the sample that has a concentration of 10 g L^{-1}. This suggests that, at this concentration (10 g L^{-1}), the network has a larger number of elastically active links that result in larger maximum values of G'. Samples prepared at 70 °C exhibit a similar trend but the final values of G' are lower than those obtained for samples prepared at 37 °C. In addition, T_G gradually shifts to higher temperatures as fibrinogen concentrations increase (see arrows in Fig. 5b). Fig. 6 shows the values of the elastic modulus G' at 70 °C as a function of fibrinogen concentration obtained from temperature sweeps (Fig. 5). It is evident from this figure that, for both preparation temperatures, the elastic modulus shows a power-law decrease when fibrinogen concentrations increase. On the other hand, samples prepared at 37 °C decrease more rapidly than samples

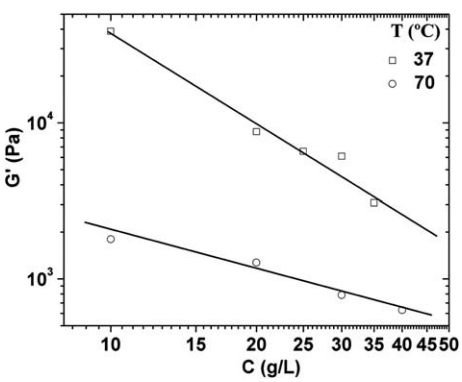

Fig. 6 Elastic modulus at 70 °C obtained in the temperature sweeps as a function of fibrinogen concentration for samples prepared at 37 °C and 70 °C. Experiments were performed at a strain of 0.025% and at $\omega = 10$ rad per s.

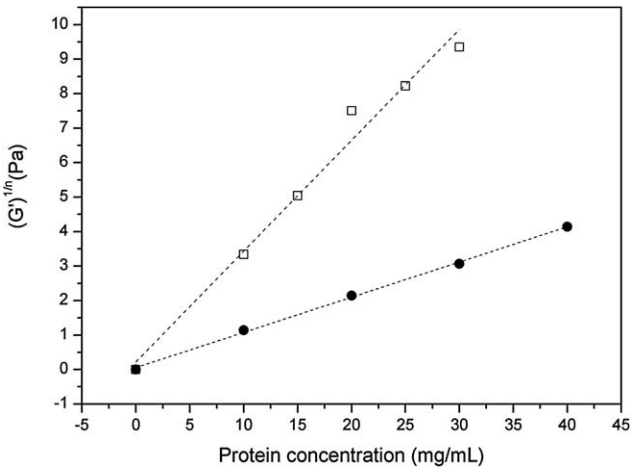

Fig. 7 Protein concentration dependence of G' values for fibrinogen gels.

prepared at 70 °C. This means that increasing the fibrinogen concentration and the preparation temperature can both affect the number of effective crosslinks in the final network and cause a decrease in the elastic modulus. Again this is related to the degrees of freedom of αC domains, which decrease with protein concentration (due to lack of space) and temperature (conformational changes in the protein structure).

Of particular interest is the influence of microstructure on the mechanical behavior of the gels. In order to characterize this, a considerable amount of work has been undertaken to arrive at a generic description of gel elasticity, based on percolation[35] and fractal theories.[36] Linden and Sagis[37] found that most data can be described by one percolation model and scaling exponent (n) that can be determined by a graphical method. This method uses a plot of $(G')^{1/n}$ *versus* c, and extrapolates it to zero modulus. This procedure makes use of the fact that, independently of the value of n, all curves must intersect the concentration axis at the same value. When the assumed value of n is close to the actual value, such a plot will be linear. If n is too small or too large the plots are curved. From plots of $(G')^{1/n}$ *versus* c for various n (Fig. 7), the n values that give an approximately straight line were selected. These values of G' were obtained in the linear viscoelastic regime, where G' is independent of the applied strain. The exponent n, which is a function of the gel structure, had values of 2.5 and 4.3 for fibrinogen hydrogels formed at 37 °C and 70 °C respectively. These values are higher than the typical exponent for linear particles ($n < 2.5$).[38,39] This suggests that the aggregates are either branched or organized into large clusters with a low density.

Further analysis concerns the evaluation of projected images (SEM images) of the gels. Fig. 8 shows examples of the hydrogels prepared under different process conditions. Both processes evaluated (37 and 70 °C) produce an isotropic macroporous hydrogel that exhibits a classic, uniform morphology in scanning electron microscopy (SEM) micrographs. Some artifacts have been found that are attributed to the dehydration of samples for SEM analysis. However, the pore structure of the gels is still evident and similar to those of gels synthesized with polyethylene glycol and polylysine[10] and polyvinyl alcohol with chitosan.[40] Fig. 8 also shows similar patterns for both hydrogels. The two gels exhibit an open 3D and homogeneous network structure with large pores. However, hydrogels synthesized at 70 °C exhibit a more heterogeneous pore size distribution. This fact is clearly related to the temperature used for the formation of the hydrogels. When the protein loses its native structure, it results in rapid aggregation and formation of non-homogeneous microstructures resulting in gels with variable pore sizes.[41] Histograms of the average pore diameters were generated (Fig. 9) from different SEM images for hydrogels formed at both temperatures. The histograms illustrate that there are significant differences in the average pore diameter and distribution between both synthesis protocols. There is a significant increase in the average pore diameter (obtained from the mode of the pore size distribution) from 210 to 317 nm with increasing synthesis temperature. On the other hand, the pore size distribution of the gel synthesized at 37 °C is unimodal. Meanwhile, the distribution corresponding to samples prepared at 70 °C is observed to be bimodal which can be explained by the large volume of interconnected pores. However, the most significant difference between both hydrogels is the wall thickness. It can be observed that an increase in the synthesizing temperature causes the hydrogel wall thickness to increase about ten times. The probable reason for the wall changes with temperature is the higher tendency of unfolded fibrinogen molecules to form fibers.

Also, a fractal dimension can be quantified from SEM images of the gels. To do this, the box counting method was applied to different SEM images. This protocol consists of applying an increasingly fine grid over the area studied and counting, at each iteration, the number of boxes containing at least one part of the

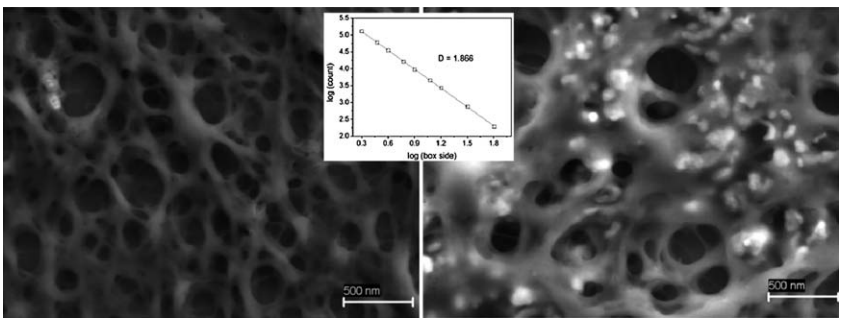

Fig. 8 SEM images of fibrinogen gels (20 g L^{-1}) formed at 37 °C (left) and 70 °C (right). The inset shows the log of the box size *vs.* the log of the pixel count.

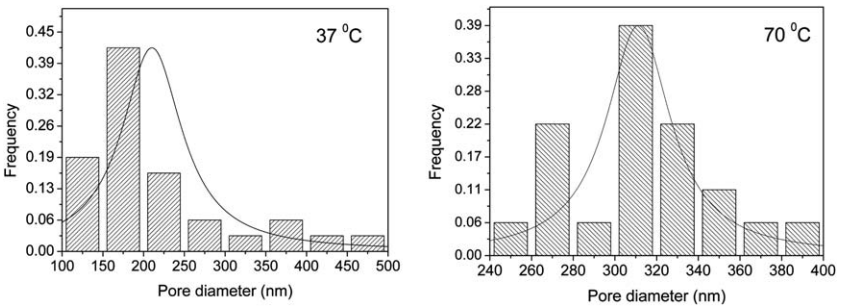

Fig. 9 Pore diameter distribution from different pictures of fibrinogen hydrogels synthesized at 37 °C (left) and 70 °C (right).

object to be measured. The fractal dimension D_f is then linked to the number $n(s)$ of boxes of dimension s necessary to fill the surface area of the particle according to:[42]

$$D_f = \lim_{s \to 0} \frac{\ln n(s)}{\ln (1/s)} \quad (2)$$

This method was also optimized by means of a calculation procedure stemming from the work of Foroutan-Pour *et al.*,[43] which allows a precise determination of the key parameters of the method, namely the number and the dimensions of the boxes.[44] The images, initially with 256 grey levels and 1024 × 768 pixels in size, are converted to binary images. The fractal dimension is then derived from the slope of a least-square linear fit of the plot of log n *versus* log (box size), where n is the number of non-overlapping equal boxes that would fill the projected surface area of the aggregate. This operation can be carried out by different software packages.[45] Log–log representations of the calculations of fractal dimension on the systems studied are shown in Fig. 8. The procedure leads to values of $D_f = 1.866$ and $D_f = 1.862$ for hydrogels synthesized at 37 and 70 °C, respectively. These values are quite close to those found for fibrin gels.[33,34] Most authors, based on Minkowski–Bouligand dimension and the contents of projections on the directions of the planes, have demonstrated that, in general, there is no general relationship between 3D and 2D fractal dimensions.[46] However, functional relationships between 2D and 3D fractal dimensions were found for specific systems, such as aluminum oxide nanoparticles,[47] assuming a uniform mass distribution of the object along the third dimension: $d_{3D} = 0.47d_{2D} + 1.78$. This relationship works well for hydrogels synthesized at 37 °C, but not for those synthesized at 70 °C. Probably, the temperature-induced conformational changes of fibrinogen result in a non-uniform mass distribution along the third dimension in these samples.

Biotemplating of silica architectures

Using sodium silicate as the source of silica, mineralization *via* condensation was investigated on fibrinogen hydrogels. By adjusting the solution to a pH of 3.0, the silica condensation was initiated and confined to the hydrogel templates. Hydrogel-directed silica condensation was complete in 12 hours by using a hydrothermal treatment at mildly elevated temperatures (100 °C) to enhance both the diffusion rates of silica precursors (see Scheme 1) and the rate of condensation. Finally, the organic templates were removed *via* calcination at 600 °C for 7 hours in a constant air flux.

Scanning electron microscopy was used to characterize the surface morphology of the synthesized materials. Fig. 10 shows scanning electron microscopy (SEM) images of the final materials obtained with gels synthesized at 37 and 70 °C. Both series exhibit similar features but with some differences. In general, the materials show two well-defined regions: one sponge-like (≈80%) and the other with well defined ordered topologies (Fig. 10, left-hand images). We have not found variations in the distribution of areas as a function of the type of the gel.

Regarding the sponge-like materials (middle column, Fig. 10), we have calculated their fractal dimensions following the imaging procedure that was already discussed. Values of 1.8203 and 1.7936 have been obtained for the materials synthesized with gels prepared at 37 and 70 °C, respectively. Fractal dimensions of materials from gels at 37 °C agree better with the fractal dimensions of the corresponding templates than those obtained from gels at 70 °C. This fact also correlates well with conclusions from the rheological study of the templates. Hydrogels obtained at 37 °C are more resistant to deformation than those obtained at 70 °C. Consequently, this resistance to deformation results in a more reliable template.

Focusing now on the other regions of the sample, we observe the formation of long structures. When the template corresponds to gels prepared at 37 °C, we obtain polygonal fibers of different length whose width varies from 10 to 30 μm. For the gels prepared at 70 °C, the fibers are also polygonal but more homogeneous in both length and width with values between 5 and 10 μm. To explain this we must remember that the synthesis is performed through hydrothermal treatment. Essentially, the mechanism for forming these structures can be explained as follows: precipitation within the cavities of the gel results in the formation primary nanostructures that subsequently undergo oriented aggregation involving linear attachment owing to specific interactions of inorganic crystals with the protein domains leading to the growth of fibers.[48] When the template is more flexible, the resulting material presents a more homogeneous structure.

The amorphous character of these structures (data not shown) was also corroborated from high-resolution powder X-ray diffraction experiments that showed no discernible peaks. Fig. 11 also shows a high-resolution TEM micrograph, confirming that the sample is indeed fully amorphous. Among other biogenic minerals, silica appears rather singular. Carbonate and phosphate salts are crystalline, ionic or covalent solids whose precipitation is dictated by solubility equilibria. In contrast, silica is an amorphous metal oxide formed by more complex inorganic

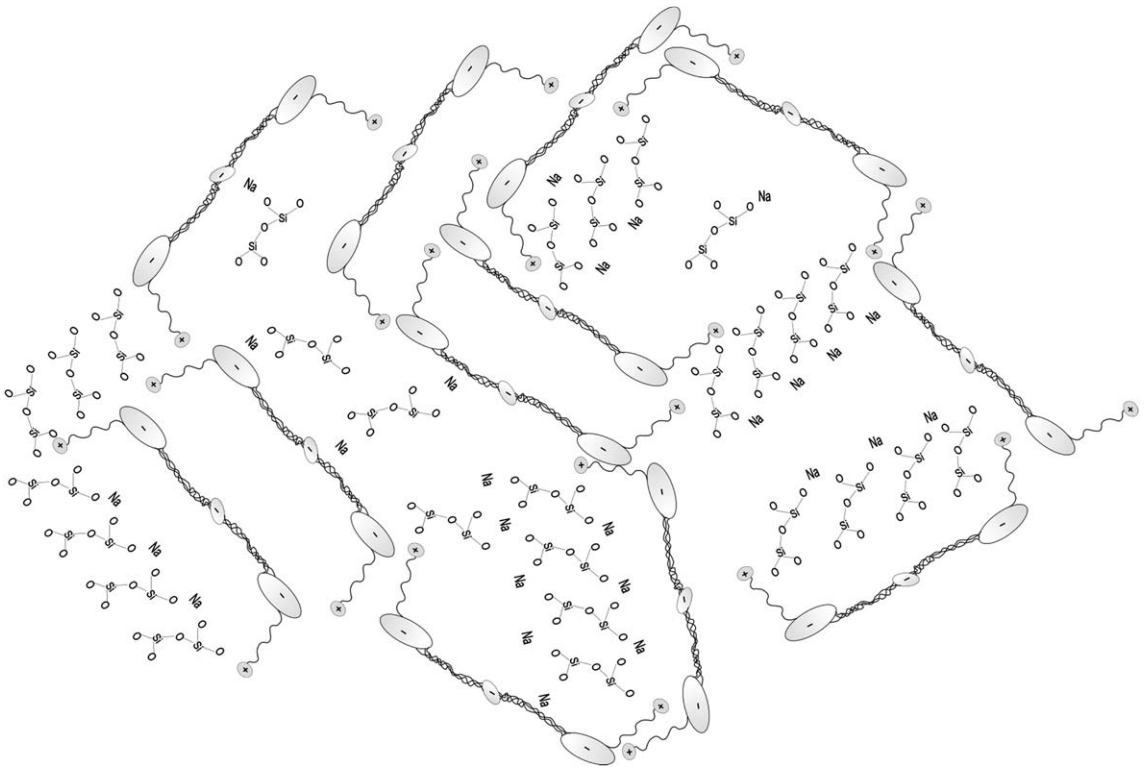

Scheme 1 Proposed mechanism for the condensation of the silica precursor in fibrinogen hydrogel.

polymerization processes.[49] Furthermore, the amorphous nature of the synthesized materials can also be related to the strong dipolar interactions between the fibrinogen molecules, which have a pronounced dipole moment,[50] and the polymorphism of the templates.[51] Previous studies have demonstrated inhibitory roles of biological macromolecules in crystallization processes.[52] Thus, we suggest that fibrinogen molecules and sodium ions may cooperate in the stabilization of amorphous silica.

Regarding the existence of two different topologies for sol–gel polycondensation under acidic conditions, when anionic silicate species are present in the system, the template should be composed of cationic structures or doped with an appropriate amount of cationic analogues.[53,54] At pH 3.0 fibrinogen has a positive net charge (IP = 5.5). However, it still has negatively charged residues on the E and D-domains. The αC-domains, which are rich in Arg and Lys residues, are mostly positively charged. During the silica polycondensation process, the αC-domains, which tend to be non-covalently tethered to the E-domains, disconnect to interact with the silicic acid.[55] Literature reports indicate that fibrinogen adsorption on 2D solid surfaces occurs in a similar way and basically in two different orientations: "side-on" (laying on the surface) and "end-on"

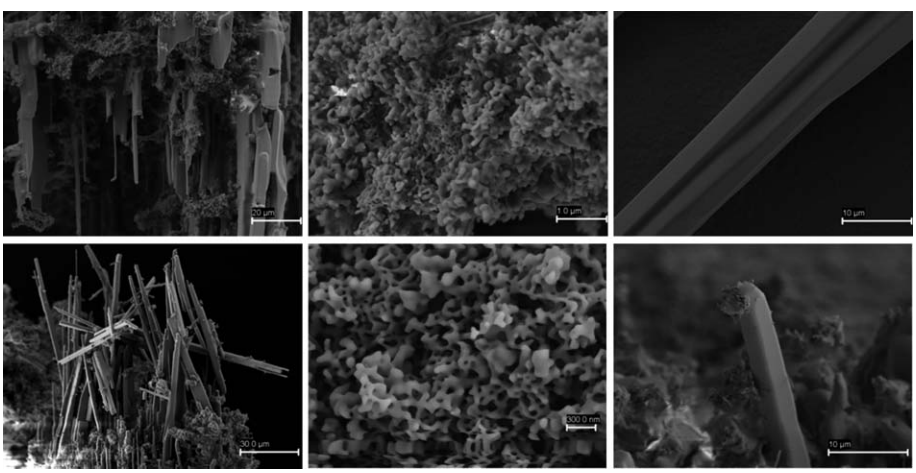

Fig. 10 SEM images of the various morphologies present in templated silica structures prepared from gels formed at 37 °C (upper set) and from gels formed at 70 °C (lower set).

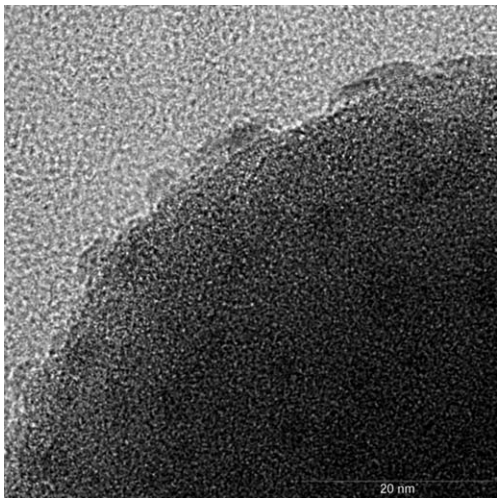

Fig. 11 High-resolution TEM image of a templated silica sample, confirming that it is entirely amorphous.

(standing on the surface).[56] Thus, we propose here a similar path for condensation where the stochastic interactions of inorganic precursors and the template lead to the formation of two different structures. Interactions through a side-end molecular orientation favors lateral interactions generating large fibers. In contrast the side-on adsorption promotes equilateral interaction and therefore the formation of bicontinuous structures.

4. Conclusions

In this study we have investigated a new route for the formation of silica nanostructures in bioinspired templates. These templates were obtained by incubation of fibrinogen under acidic conditions at 37 and 70 °C. Both hydrogels exhibit similar topologies with variable pore size distributions and stiffness. The origin of these variations seems to be governed by the different strength of association of fibrinogen molecules below (37 °C) and above (70 °C) the denaturation temperatures. The biotemplate was completely removed after calcination leading to the formation of amorphous silica with two different nanostructures: sponge-like (normal interactions) and polygonal fibers (parallel interactions). We conclude that the source of these two structures lies on the anisotropic shape of the fibrinogen molecule, which results in stochastic interactions with the inorganic precursor. Also, as a consequence of gel stiffness, sponge-like structures from hydrogels at 37 °C exhibited a good replica of the integral structure of the original template. In the end, the simplicity and environmental compatibility of this bioinspired templating method makes it useful for scale-up manufacturing of inorganic nanostructures.

Acknowledgements

The authors acknowledge Xunta de Galicia (project no. 10PXIB206258PR), Universidad Nacional del Sur, Concejo Nacional de Investigaciones Científicas y Técnicas de la República Argentina (CONICET, PIP-11220100100072), and Education Audiovisual Culture, Executive Agency European Commission (EMUNDUS18) for their financial support.

References

1 P. Fratzl, *J. R. Soc., Interface*, 2007, **4**, 637.
2 N. Kröger, S. Lorenz, E. Brunner and M. Sumper, *Science*, 2002, **298**, 584.
3 S. Reuveni, R. Granek and J. Klafter, *Phys. Rev. Lett.*, 2008, **100**, 208101.
4 W. Min, G. Luo, B. J. Cherayil, S. C. Kou and X. S. Xie, *Phys. Rev. Lett.*, 2005, **94**, 198302.
5 M. B. Enright and D. M. Leitner, *Phys. Rev. E: Stat., Nonlinear, Soft Matter Phys.*, 2005, **71**, 011912.
6 S. Reuveni, R. Granek and J. Klafter, *Proc. Natl. Acad. Sci. U. S. A.*, 2010, **107**, 13696.
7 Q. Dong, H. Su, J. Xu, D. Zhang and R. Wang, *Mater. Lett.*, 2007, **61**, 2714.
8 U.-J. Kim, J. Park, C. Li, H.-J. Jin, R. Valluzzi and D. L. Kaplan, *Biomacromolecules*, 2004, **5**, 786.
9 P. Mohanty, D. Li, T. Liu, Y. Fei and K. Landskron, *J. Am. Chem. Soc.*, 2009, **131**, 2764.
10 G. R. Souza, E. Yonel-Gumruk, D. Fan, J. Easley, R. Rangel, L. Guzman-Rojas, J. H. Miller, W. Arap and R. Pasqualini, *PLoS One*, 2008, **3**, e2242.
11 J. H. Brown, N. Volkmann, G. Jun, A. H. Henschen-Edman and C. Cohen, *Proc. Natl. Acad. Sci. U. S. A.*, 2000, **97**, 85.
12 S. Yakovlev and L. Medved, *Biochemistry*, 2009, **48**, 5171.
13 G. Tsurupa, R. R. Hantgan, R. A. Burton, I. Pechik, N. Tjandra and L. Medved, *Biochemistry*, 2009, **48**, 12191.
14 N. Hassan, L. R. S. Barbosa, R. Itri and J. M. Ruso, *J. Colloid Interface Sci.*, 2011, **362**, 118.
15 N. Hassan, J. Maldonado-Valderrama, A. P. Gunning, V. J. Morris and J. M. Ruso, *Colloids Surf., B*, 2011, **87**, 489.
16 N. Hassan, J. Madonado-Vaderrama, A. P. Gunning, V. J. Morris and J. M. Ruso, *J. Phys. Chem. B*, 2011, **115**, 6304.
17 N. Hassan, J. M. Ruso and P. Somasundaran, *Colloids Surf., B*, 2011, **82**, 581.
18 C. Y. Khripin, D. Pristinski, D. R. Dunphy, C. J. Brinker and B. Kaehr, *ACS Nano*, 2011, **5**, 1401.
19 E. Gianotti, U. Diaz, S. Coluccia and A. Corma, *Phys. Chem. Chem. Phys.*, 2011, **13**, 11702.
20 A. C. Fournier and K. M. McGrath, *Soft Matter*, 2011, **7**, 4918.
21 G. Wei, J. Reichert, J. Bossert and K. D. Jandt, *Biomacromolecules*, 2008, **9**, 3258.
22 K. Ako, T. Nicolai and D. Durand, *Biomacromolecules*, 2010, **11**, 864.
23 J. D. Ferry, *The Viscoelastic Properties of Polymers*, Wiley, New York, 1980.
24 O. Robles-Vásquez, S. Corona-Galván, J. F. A. Soltero, J. E. Puig, S. B. Tripodi, E. Vallés and O. Manero, *J. Colloid Interface Sci.*, 1993, **160**, 65.
25 J. F. A. Soltero, F. Bautista, E. Pecina, J. E. Puig, O. Manero, Z. Proverbio and P. C. Schulz, *Colloid Polym. Sci.*, 2000, **278**, 37.
26 A. E. Bell, in *Water and Food Quality*, ed. T. M. Hardman, Elsevier Applied Science, Essex, 1989.
27 W. B. Yoon, S. Gunasekaran and J. W. Park, *J. Food Sci.*, 2004, **69**, 338.
28 A. Clark and S. Ross-Murphy, in *Biopolymers*, Springer, Berlin/Heidelberg, 1987, vol. 83, p. 57.
29 F. C. MacKintosh, J. Käs and P. A. Janmey, *Phys. Rev. Lett.*, 1995, **75**, 4425.
30 K. M. Weigandt, D. C. Pozzo and L. Porcar, *Soft Matter*, 2009, **5**, 4321.
31 B. Ozbas, K. Rajagopal, J. P. Schneider and D. J. Pochan, *Phys. Rev. Lett.*, 2004, **93**, 268106.
32 S. K. Kundu, M. Yoshida and M. Shibayama, *J. Phys. Chem. B*, 2010, **114**, 1541.
33 Y. Lin, J. Wang, L.-J. Wan and X.-H. Fang, *Ultramicroscopy*, 2005, **105**, 129.
34 M. Yaseen, X. Zhao, A. Freund, A. M. Seifalian and J. R. Lu, *Biomaterials*, 2010, **31**, 3781.
35 D. Stauffer, A. Coniglio and M. Adam, *Adv. Polym. Sci.*, 1982, **44**, 103.
36 W.-H. Shih, W. Y. Shih, S.-I. Kim, J. Liu and I. A. Aksay, *Phys. Rev. A: At., Mol., Opt. Phys.*, 1990, **42**, 4772.
37 E. van der Linden and L. M. C. Sagis, *Langmuir*, 2001, **17**, 5821.
38 R. H. Colby and M. Rubinstein, *Macromolecules*, 1990, **23**, 2753.
39 K. Kroy and E. Frey, *Phys. Rev. Lett.*, 1996, **77**, 306.

40 C. Pecharromán, F. Esteban-Betegón, J. F. Bartolomé, G. Richter and J. S. Moya, *Nano Lett.*, 2004, **4**, 747.
41 W. Ho, B. Tawil, J. C. Y. Dunn and B. M. Wu, *Tissue Eng.*, 2006, **12**, 1587.
42 A. Giorgilli, D. Casati, L. Sironi and L. Galgani, *Phys. Lett. A*, 1986, **115**, 202.
43 K. Foroutan-pour, P. Dutilleul and D. L. Smith, *Appl. Math. Comput.*, 1999, **105**, 195.
44 S. Bau, O. Witschger, F. Gensdarmes, O. Rastoix and D. Thomas, *Powder Technol.*, 2010, **200**, 190.
45 N. Ibaseta and B. Biscans, *Powder Technol.*, 2010, **203**, 206.
46 H. Akkari, I. Bhouri, P. Dubois and M. H. Bedoui, *Math. Model. Nat. Phenom.*, 2008, **3**, 48.
47 S. Ganguly, S. Basu and S. Sikdar, *Proc. Inst. Mech. Eng., Part N*, 2012, **226**, 3.
48 N. Hassan, V. Verdinelli, J. M. Ruso and P. V. Messina, *Langmuir*, 2011, **27**, 8905.
49 D. M. Nelson, P. Tréguer, M. A. Brzezinski, A. Leynaert and B. Quéguiner, *Global Biogeochem. Cycles*, 1995, **9**, 359.
50 V. C. Yee, K. P. Pratt, H. C. F. Côté, I. L. Trong, D. W. Chung, E. W. Davie, R. E. Stenkamp and D. C. Teller, *Structure*, 1997, **5**, 125.
51 M. Brinkmann, G. Gadret, M. Muccini, C. Taliani, N. Masciocchi and A. Sironi, *J. Am. Chem. Soc.*, 2000, **122**, 5147.
52 J. Aizenberg, G. Lambert, S. Weiner and L. Addadi, *J. Am. Chem. Soc.*, 2001, **124**, 32.
53 J. H. Jung, Y. Ono and S. Shinkai, *Chem.–Eur. J.*, 2000, **6**, 4552.
54 J. H. Jung, Y. Ono, K. Hanabusa and S. Shinkai, *J. Am. Chem. Soc.*, 2000, **122**, 5008.
55 M. W. Mosesson, *J. Thromb. Haemostasis*, 2005, **3**, 1894.
56 Z. Adamczyk, J. Barbasz and M. Cieśla, *Langmuir*, 2011, **27**, 6868.

